

Spikformer V2: Join the High Accuracy Club on ImageNet with an SNN Ticket

Zhaokun Zhou, Kaiwei Che, Wei Fang, Keyu Tian, Yuesheng Zhu, *Senior Member, IEEE*,
Shuicheng Yan, *Fellow, IEEE*, Yonghong Tian, *Fellow, IEEE*, and Li Yuan

Abstract—Spiking Neural Networks (SNNs), known for their biologically plausible architecture, face the challenge of limited performance. The self-attention mechanism, which is the cornerstone of the high-performance Transformer and also a biologically inspired structure, is absent in existing SNNs. To this end, we explore the potential of leveraging both self-attention capability and biological properties of SNNs, and propose a novel Spiking Self-Attention (SSA) and Spiking Transformer (Spikformer). The SSA mechanism eliminates the need for softmax and captures the sparse visual feature employing spike-based Query, Key, and Value. This sparse computation without multiplication makes SSA efficient and energy-saving. Further, we develop a Spiking Convolutional Stem (SCS) with supplementary convolutional layers to enhance the architecture of Spikformer. The Spikformer enhanced with the SCS is referred to as Spikformer V2. To train larger and deeper Spikformer V2, we introduce a pioneering exploration of Self-Supervised Learning (SSL) within the SNN. Specifically, we pre-train Spikformer V2 with masking and reconstruction style inspired by the mainstream self-supervised Transformer, and then finetune the Spikformer V2 on the image classification on ImageNet. Extensive experiments show that Spikformer V2 outperforms other previous surrogate training and ANN2SNN methods. An 8-layer Spikformer V2 achieves an accuracy of 80.38% using 4 time steps, and after SSL, a 172M 16-layer Spikformer V2 reaches an accuracy of 81.10% with just 1 time step. To the best of our knowledge, this is the first time that the SNN achieves 80+% accuracy on ImageNet. The code will be available at [Spikformer V2](#).

Index Terms—Spiking Neural Network, Vision Transformer, Self-Supervised Learning, Image Classification

1 INTRODUCTION

Human brains with incredible efficiency and the ability to perform complex pattern recognition tasks have been objects of imitation and sources of innovation for deep Artificial Neural Networks (ANNs). In recent years, deep learning has developed rapidly with ANNs and achieved remarkable success in many fields, including natural language processing [1], [2], [3], computer vision [4], [5], [6], and robotics [7]. Exploring how to leverage the intrinsic efficient computation paradigm of biological neural systems to implement neural networks with low power consumption is of great value. Spiking Neural Networks (SNNs) are a promising way to achieve energy-efficient intelligence, as they mimic biological neuronal behavior by using spiking signals for inter-neuron communication [8]. SNNs can run smoothly on neuromorphic chips [9], [10], [11] by only performing spike-based accumulation operations and skipping zero values of input or activation (i.e., event-driven) [12], [13], which consume much less power than ANNs.

Training large-scale SNNs to achieve competitive performance in real-world pattern recognition tasks still presents a significant challenge. Some works attempt to build larger-

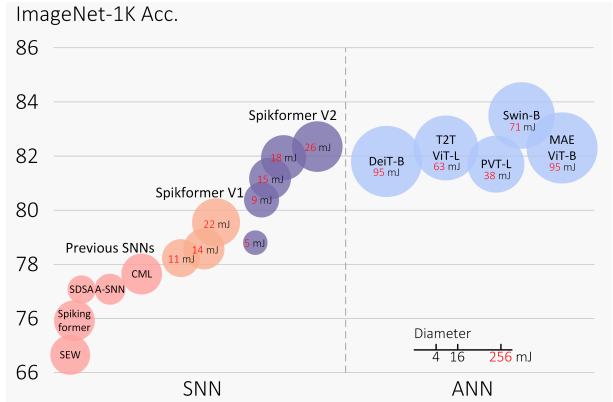


Fig. 1: ImageNet-1K classification results for ● previous SNNs, ● Spikformer V1, ● Spikformer V2 and ● Vision Transformers. The diameter of each bubble is logarithmically proportional to the theoretical energy consumption. We demonstrate that the Spikformer V2 can achieve equivalent classification accuracy levels to those of ANN-Transformers, while maintaining lower theoretical energy consumption.

- Zhaokun Zhou, Kaiwei Che, Yuesheng Zhu, Yonghong Tian and Li Yuan are with Peking University, School of Electronic and Computer Engineering, Shenzhen Graduate School, China, and also with PengCheng Laboratory. E-mail: {zhouzhaokun, chekaiwei}@stu.pku.edu.cn, and {zhuy, yhtian, yuanli-ec}@pku.edu.cn.
- Wei Fang is with Peking University, School of Computer Science, China, and also with PengCheng Laboratory. E-mail: fwei@pku.edu.cn.
- Keyu Tian is with Peking University, Center for Data Science, China. E-mail: keyutian@stu.pku.edu.cn.
- Shuicheng Yan is with Beijing Academy of Artificial Intelligence. E-mail: shuicheng.yan@gmail.com.

Manuscript received August 31, 2023.

scale networks from various perspectives, including the design of spiking residual networks [14], [15], attention mechanisms [16], spiking neuron designs [17], [18]. However, in ANNs, as shown in Fig. 1, the classification accuracy on ImageNet [19] generally exceeds 80% [20], [21], [22], [23], [24], [25], [26], with the highest reaching 91.1% [27]. The existing directly trained pure SNNs usually achieve below 80% [14], [15], [28], with the highest being 78.46% [29]. To overcome the bottleneck, we need to construct more

powerful and efficient SNN. Self-attention can select interest information by modeling both long and short dependencies of input features, enabling Transformer to flourish in various domains of deep learning, including Natural Language Processing (NLP) [1], [33], computer vision [4], [23], [25], and large language/vision models [2], [3], [6]. However, the exploration of self-attention mechanisms in SNNs is still absent. Given the biological inspiration behind these two mechanisms and the excellent performance of self-attention, applying self-attention to SNNs for more advanced deep learning is an intriguing avenue to explore.

However, integrating the self-attention mechanism into SNNs is not straightforward. Vanilla Self-Attention (VSA) [33] consists of three components: Query, Key, and Value. As illustrated in Fig. 2 (a), The standard procedure of VSA computes a floating-point matrix through Query and Key dot product, followed by softmax normalization (involving exponentiation and division) to create the attention map for Value scaling. These steps clash with the computational characteristics of SNNs, i.e., multiplication avoidance. Furthermore, the high computational cost of VSA (dense floating-point calculations) makes it impractical to apply to SNNs directly. Hence, to enable Transformer on SNNs, we require a new self-attention variant that is effective, computation-efficient, and multiplication-free. We thus propose Spiking Self-Attention (SSA), as shown in Fig. 2 (b). SSA is the first to apply the self-attention mechanism to SNNs, capturing interdependence using spike sequences. In SSA, the Query, Key, and Value are in spike form which only consists of 0 and 1. The challenges to the adoption of self-attention in SNNs are mainly due to softmax. As depicted in Fig. 2, the attention map computed from spike-form Query and Key has inherent non-negativeness, filtering out irrelevant features. Therefore, we do not require the softmax to ensure the non-negative attention matrix, which is its primary role in VSA [34]. Table 1 demonstrates that our SSA is comparable to VSA in the effect of processing spike sequences. Based on these insights, we eliminate softmax normalization for the attention map in SSA. Some prior Transformer variants also eliminate softmax or substitute it with a linear function. For instance, in Performer [35], the positive random feature is used to approximate softmax; CosFormer [34] replaces softmax with ReLU and cosine function.

The sparse spike-form Query, Key, and Value in SSA are computed through logical AND operations and addition without involving multiplications, resulting in efficiency due to sparsity and simplified operations. Based on the SSA, we propose the Spiking Transformer (Spikformer). Fig. 3 shows the overview of Spikformer. It attains high performance on both static and neuromorphic datasets. To the best of our knowledge, this is the first work to investigate the self-attention and directly-training Transformer in SNNs.

Despite the improvement over previous SNNs, Spikformer still lags significantly behind ANN performance on ImageNet. Two common approaches to enhancing Spikformer performance are optimizing network architecture and improving learning methods. Regarding architecture improvement, we eliminate the max-pooling in Spike Patch Splitting module that might cause information loss and blur features. Inspired by the substantial benefits of early-stage injection of convolutional induced biases in ANN Vision

Transformer (ViT) [36], we explore the significance of shallow convolutions in SNN-Transformer and the impact of the number of convolution layers on model performance, as depicted in Fig. 4. The redesigned patch splitting module is referred to as the Spiking Convolutional Stem (SCS) and the Spikformer based on SCS is named Spikformer V2.

Despite the performance improvement achieved by Spikformer V2, we observe that training becomes unstable and performance degrades when Spikformer V2 exceeds more than 12 layers. To obtain larger and deeper Spikformer V2, we investigate the masked image modeling [5], [37], a Self-Supervised Learning method that demonstrates efficient and stable training on large ANN-Transformers. However, Self-Supervised Learning, an important learning mode in the brain [38], [39], has not been extensively studied in SNNs. We pre-train Spikformer V2 with Mask Autoencoder style [5]. We use the standard ANN-Transformer as a decoder to better reconstruct the masked images and obtain a powerful Spikformer V2. Note that using the ANN-Transformer decoder does not affect Spikformer V2 as a pure SNN. It will be discarded after pre-training, and only the Spikformer V2 will be used for subsequent fine-tuning. With SSL, we can train larger and deeper Spikformer V2, which further unleashes the potential of SSA and Spikformer V2 and elevate their performance upper bound.

As shown in Fig. 1, after supervised training, Spikformer V2-8-512 attains an accuracy of 80.38% across 4 simulation time steps. Based on self-supervised pre-training, Spikformer V2-16-768 achieves 81.10% accuracy on ImageNet with only 1 time step. To the best of our knowledge, this is the first time that SNNs surpass 80% on ImageNet. This further emphasizes the potential of large-scale SNNs to achieve high performance, in addition to their biocompatibility and computational efficiency.

The rest of this paper is structured as follows. Sec. 2 introduces the background and related work. Next, we review Spikformer and its components, particularly Spiking Self-Attention, in Sec. 3. We provide a detailed description of Spikformer V2 in Sec. 4. Subsequently, we present the experimental results in Sec. 5. Finally, we conclude and discuss future work in Sec. 6.

2 BACKGROUND AND RELATED WORK

Vision Transformers. Transformers, initially designed for NLP tasks [1], [33], have demonstrated impressive performance in computer vision, including image classification [4], [22], object detection [25], [40], [41], semantic segmentation [23], [24], and low-level image processing [26]. In the context of image classification, a conventional ViT [4] architecture comprises three main components: a patch splitting module, transformer encoder layers, and a linear classification head. The transformer encoder layer encompasses a self-attention block and a multi-perception layer block. Self-attention is a fundamental component that plays a crucial role in the success of ViT. It assigns weights to the feature Values of image patches based on the dot-product of Query and Key, followed by a softmax function. It enables the model to capture global dependencies and represent important patterns of interest in the input data [34], [42]. Several studies have explored enhancements to the structure of ViT. One notable

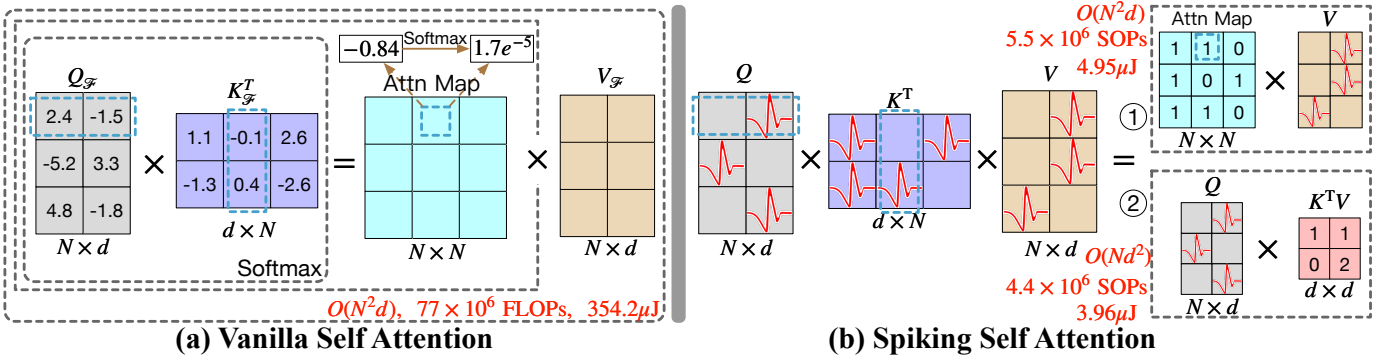


Fig. 2: Comparison between Vanilla Self-Attention (VSA) and our Spiking Self-Attention (SSA). A red spike indicates a value of 1 at a specific location. The blue dashed boxes demonstrate examples of matrix dot product operations. For simplicity, we select one of the heads of SSA, where N represents the number of input patches and d denotes the feature dimension of one head. FLOPs stands for floating-point operations, and SOPs represents the theoretical synaptic operations. The theoretical energy consumption for performing one calculation between Query, Key, and Value in one time step is derived from the 8-encoder-blocks 512-embedding-dimension Spikformer on the test set of ImageNet, using the method in [30], [31], [32]. (a) In VSA, $Q_{\mathcal{F}}, K_{\mathcal{F}}, V_{\mathcal{F}}$ are in float-point forms. After the dot-product of $Q_{\mathcal{F}}$ and $K_{\mathcal{F}}$, the softmax function regularizes the attention map values to be positive. (b) In SSA, all values in the attention map are non-negative and the computation is sparse using spike-form Q, K, V (5.5×10^6 VS. 77×10^6 in VSA). As a result, SSA consumes less energy compared to VSA ($354.2\mu\text{J}$). The SSA is decomposable (the calculation order of Q, K and V is changeable).

improvement is the utilization of convolution layers for patch splitting, which has demonstrated the ability to expedite convergence and mitigate the data-intensive nature of ViT [36], [43]. Subsequent studies, such as PVT [44], Swin [45], and MViTv2 [46], have integrated the pyramid structure with transformers and eliminated the class token originally present in the architecture. Various approaches are proposed to address the computational complexity of self-attention and enhance its capacity to model visual dependencies [35], [47], [48], [49]. In this study, we specifically investigate the efficacy of self-attention in SNNs and aim to develop a powerful Spiking Transformer for image classification.

Self-Supervised Learning. In ANNs, Self-Supervised Learning (SSL) has emerged as a promising paradigm for both computer vision and natural language processing [1], [5], [37]. Contrastive learning and mask auto-encoding are two mainstream SSL. Contrastive learning [50], [51], [52], [53] aims to learn invariances by comparing augmented views of unlabeled images. Mask auto-encoding enables the learning of robust representations by reconstructing masked inputs using simple data augmentation techniques [1], [5], [37]. BEiT [37] pioneered the integration of mask auto-encoding into the computer vision community, while MAE [5] further refined this approach by introducing an asymmetric encoder and decoder architecture. In MAE, the encoder selectively bypasses masked tokens to alleviate computational burden, while the decoder processes all tokens. We will explore mask auto-encoding in SNNs for the first time.

Spiking Neural Networks. In contrast to conventional deep learning models that utilize continuous decimal values to represent information, SNNs employ discrete spike sequences for computation and information transmission. Spiking neurons, such as the Leaky Integrate-and-Fire (LIF) neuron [54], PLIF [17], and others, are capable of converting continuous input signals into spike sequences. There are two approaches to obtaining deep SNN models: ANN-to-SNN

conversion and direct training. In the process of ANN-to-SNN conversion [55], [56], [57], [58], [59], [60], the ReLU activation layers in a high-performance pre-trained ANN are replaced with spiking neurons to obtain an equivalent SNN model. The converted SNN requires a larger number of time steps to accurately approximate the ReLU activation function, resulting in increased latency [61]. In the field of direct training [14], [62], SNNs are unfolded over a series of simulation time steps and trained using a variant of the back-propagation through time algorithm [63], [64]. Due to the non-differentiable nature of the event-triggered mechanism in spiking neurons, surrogate gradients are employed for back-propagation [65], [66]. In [67], implicit differentiation on the equilibrium state is adopted to train SNNs. Various models originally developed for ANNs have been successfully transferred to SNNs. However, the investigation of self-attention in SNNs remains an open research area. Convolution-based temporal attention was proposed as a means to reduce unnecessary time steps in SNNs [16]. Both [68], [69] employ ANN-Transformer architectures for spike data processing, despite their titles containing “Spiking Transformer”. [70] presents an ANN-SNN conversion Transformer, but it still utilizes vanilla self-attention. In this study, we aim to investigate the feasibility of integrating self-attention and Transformer into SNNs.

3 SPIKFORMER

We introduce Spiking Transformer (Spikformer), a pure SNN that integrates the self-attention and Transformer for improved learning capability. Next, we present the overview and components of Spikformer in detail.

3.1 Overall Architecture

Fig. 3 shows the structure and components of Spikformer. The Spiking Patch Splitting (SPS) module converts a 2D

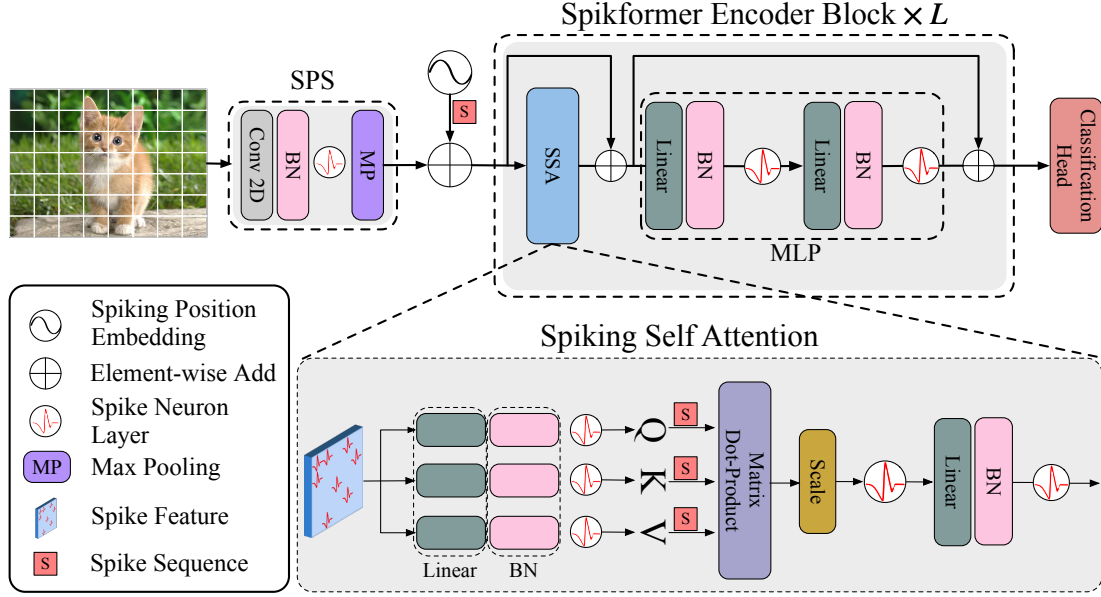


Fig. 3: The architecture of Spiking Transformer (Spikformer) includes a spiking patch splitting module (SPS), a Spikformer encoder, and a Linear classification head. We observe that layer normalization (LN) is not suitable for SNNs, hence we empirically utilize batch normalization (BN) instead.

image sequence $I \in \mathbb{R}^{T \times C \times H \times W}^1$ into a D dimensional spike-form feature vector and segments it into a sequence of N flattened spike-form patches x using linear projections. SNNs do not support float-point-form position embedding. We use a conditional position embedding generator [71] to produce spike-form relative position embedding (RPE) and add the RPE to patches sequence x to obtain X_0 . The conditional position embedding generator is composed of a 2D convolution layer (Conv2d) with a kernel size of 3, followed by batch normalization (BN), and a spiking neuron layer (\mathcal{SN}).

We feed the X_0 to the L -block Spikformer encoder. A Spikformer encoder block contains a Spiking Self Attention (SSA) block and a Multi-Layer Perceptron (MLP) block, similar to the standard ViT encoder block. Residual connections are used in both the SSA and MLP blocks. As the main component in Spikformer encoder block, SSA provides an efficient way to model the local-global information of images using spike-form Query (Q), Key (K), and Value (V) without softmax, which will be discussed in detail in Sec. 3.3. A Global Average-Pooling (GAP) is applied to the processed feature from Spikformer encoder and outputs the D dimensional feature which will be sent to the fully-connected-layer Classification Head (CH) to output the prediction Y . Spikformer can be expressed as follows:

$$x = \text{SPS}(I), I \in \mathbb{R}^{T \times C \times H \times W}, x \in \mathbb{R}^{T \times N \times D}. \quad (1)$$

$$\text{RPE} = \mathcal{SN}(\text{BN}(\text{Conv2d}(x))), \text{RPE} \in \mathbb{R}^{T \times N \times D}. \quad (2)$$

$$X_0 = x + \text{RPE}, X_0 \in \mathbb{R}^{T \times N \times D}. \quad (3)$$

1. The data shape in the neuromorphic dataset is $I \in \mathbb{R}^{T \times C \times H \times W}$, where T , C , H , and W represent time step, channel, height and width, respectively. A 2D image $I_s \in \mathbb{R}^{C \times H \times W}$ in static datasets has to be duplicated T times to form a sequence of images.

$$X'_l = \text{SSA}(X_{l-1}) + X_{l-1}, X'_l \in \mathbb{R}^{T \times N \times D}, l = 1 \dots L. \quad (4)$$

$$X_l = \text{MLP}(X'_l) + X'_l, X_l \in \mathbb{R}^{T \times N \times D}, l = 1 \dots L. \quad (5)$$

$$X_0 = x + \text{RPE}, X_0 \in \mathbb{R}^{T \times N \times D}. \quad (6)$$

3.2 Spiking Patch Splitting (SPS)

As shown in Fig. 3, the Spiking Patch Splitting (SPS) module is designed to transform an image into a spike-form feature of dimension D and segment it into fixed-size patches. Multiple blocks can be included in the SPS module. Following the convolutional stem in Vision Transformer [36], [43], we employ a convolution layer in each block of SPS to inject inductive bias into Spikformer. Specifically, for an image sequence $I \in \mathbb{R}^{T \times C \times H \times W}$:

$$x = \mathcal{MP}(\mathcal{SN}(\text{BN}(\text{Conv2d}(I))))), \quad (7)$$

where the 2D convolution layer (stride-1, 3×3 kernel size) and max-pooling are represented by Conv2d and \mathcal{MP} , respectively. The SPS module can consist of more than 1 block. When there are multiple SPS blocks, the output channels of the convolution layers are exponentially increased until they equal the patch embedding dimension. For example, for an output embedding dimension D and a four-block SPS module, the output channels of the four convolution layers are $D/8, D/4, D/2, D$. The 2D-max-pooling layer is applied to reduce the feature size with a fixed size after each SPS block. After the SPS processing, I is converted into a sequence of image patches $x \in \mathbb{R}^{T \times N \times D}$.

3.3 Spiking Self Attention Mechanism (SSA)

The Spikformer encoder is the core component of the whole architecture, which comprises the Spiking Self Attention

(SSA) mechanism and MLP block. We focus on SSA, beginning with a review of vanilla self-attention (VSA). For an input feature sequence $X \in \mathbb{R}^{T \times N \times D}$, the VSA in ViT has three float-point key components, namely Query ($Q_{\mathcal{F}}$), Key ($K_{\mathcal{F}}$), and Value ($V_{\mathcal{F}}$) which are computed by learnable linear matrices $W_Q, W_K, W_V \in \mathbb{R}^{D \times D}$ and X :

$$Q_{\mathcal{F}} = XW_Q, K_{\mathcal{F}} = XW_K, V_{\mathcal{F}} = XW_V, \quad (8)$$

where \mathcal{F} indicates the float-point form. The output of vanilla self-attention can be calculated as:

$$\text{VSA}(Q_{\mathcal{F}}, K_{\mathcal{F}}, V_{\mathcal{F}}) = \text{Softmax}\left(\frac{Q_{\mathcal{F}}K_{\mathcal{F}}^T}{\sqrt{d}}\right)V_{\mathcal{F}}, \quad (9)$$

where $d = D/H$ is the feature dimension of one head and H is the head number. The transformation of the Value in float-point form ($V_{\mathcal{F}}$) to spike form (V) enables the direct use of VSA in SNNs, which can be written as:

$$\text{VSA}(Q_{\mathcal{F}}, K_{\mathcal{F}}, V) = \text{Softmax}\left(\frac{Q_{\mathcal{F}}K_{\mathcal{F}}^T}{\sqrt{d}}\right)V. \quad (10)$$

However, VSA is not compatible with SNNs for two reasons. 1) The float-point matrix multiplication of $Q_{\mathcal{F}}, K_{\mathcal{F}}$ and softmax function that involves exponential calculation and division operation, violate the computation rules of SNNs. 2) The quadratic space and time complexity of the sequence length of VSA do not satisfy the efficient computational demands of SNNs.

We introduce Spiking Self-Attention (SSA), which is more adapted to SNNs than VSA, as shown in Fig. 2(b) and the bottom of Fig. 3. The Query, Key, and Value, which are denoted by Q, K , and V respectively, are first obtained by applying learnable matrices. Then they are transformed into spiking sequences by different spike neuron layers:

$$\begin{aligned} Q &= \mathcal{SN}_Q(\text{BN}(XW_Q)), \\ K &= \mathcal{SN}_K(\text{BN}(XW_K)), \\ V &= \mathcal{SN}_V(\text{BN}(XW_V)), \end{aligned} \quad (11)$$

where $Q, K, V \in \mathbb{R}^{T \times N \times D}$. We argue that the computation process of the attention matrix should employ pure spike-form Query and Key (only containing 0 and 1). Motivated by vanilla self-attention [33], we introduce a scaling factor s to regulate the large value of the matrix multiplication result. s does not alter the property of SSA, and as shown in Fig. 3, the spike-friendly SSA is formulated as:

$$\text{SSA}'(Q, K, V) = \mathcal{SN}\left(Q K^T V * s\right). \quad (12)$$

The $\mathcal{SN}(\text{BN}(\text{Linear}(\cdot)))$ is used to transform and fuse the channel information [33]:

$$\text{SSA}(Q, K, V) = \mathcal{SN}(\text{BN}(\text{Linear}(\text{SSA}'(Q, K, V)))). \quad (13)$$

We can generalize the single-head SSA presented here to the multi-head SSA. SSA operates on each time step. As shown in Eq. (12), SSA eliminates the softmax normalization of the attention matrix in Eq. (9) and directly multiplies Q, K and V . Fig. 2(b) illustrates a simple calculation example. Our SSA does not require softmax, which actually impedes the implementation of self-attention in SNNs. According to Eq. (11), the spiking neuron layer \mathcal{SN}_Q and \mathcal{SN}_K produce the spike sequences Q and K , which are inherently non-negative (0 or 1). This leads to a non-negative attention map.

TABLE 1: Analyzing the rationality of SSA. We substitute SSA with alternative attention variants while keeping the remaining network structure in Spikformer unchanged. We show the accuracy (Acc) on CIFAR10-DVS [72], CIFAR10/100 [73]. OPs (M) is the number of operations (For $A_I, A_{\text{LeakyReLU}}, A_{\text{ReLU}}$ and A_{softmax} , OPs is FLOPs, and SOPs is ignored; For A_{SSA} , it is SOPs.) and P (μJ) is the theoretical energy consumption for a single calculation involving Q, K, V .

	CIFAR10-DVS	CIFAR10	CIFAR100
	Acc/OPs (M)/P (μJ)		
A_I	79.40/16.8/77	93.96/6.3/29	76.94/6.3/29
$A_{\text{LeakyReLU}}$	79.80/16.8/77	93.85/6.3/29	76.73/6.3/29
A_{ReLU}	79.40/16.8/77	94.34/6.3/29	77.00/6.3/29
A_{softmax}	80.00/19.1/88	94.97/6.6/30	77.92/6.6/30
A_{SSA}	80.90/0.66/0.594	95.19/1.1/0.990	77.86/1.3/1.170

SSA filters out the irrelevant information and only retains the relevant features. Hence, the softmax is not required to guarantee the non-negativeness of the attention map.

In contrast to the float-point-form $X_{\mathcal{F}}$ and $V_{\mathcal{F}}$ in ANNs, the spike form of the input X and the Value V of self-attention in SNNs has limited information content. The spike-form coarse features X, V in SNNs do not require the fine-grained modeling of VSA, which uses float-point-form $Q_{\mathcal{F}}, K_{\mathcal{F}}$ and softmax operations that are redundant and ineffective for extracting more information from X, V than SSA. That is, SSA is a more appropriate and efficient self-attention mechanism for SNNs than VSA. To verify the above observations, we compare our SSA with four other attention map computation methods in the experiments, as illustrated in Tab. 1. A_I represents the attention map derived from directly multiplying the float-points $Q_{\mathcal{F}}$ and $K_{\mathcal{F}}$, which keeps both positive and negative correlation. A_{ReLU} employs the multiplication of $\text{ReLU}(Q_{\mathcal{F}})$ and $\text{ReLU}(K_{\mathcal{F}})$ to generate the attention map. A_{ReLU} maintains the positive values of $Q_{\mathcal{F}}, K_{\mathcal{F}}$ and zeros out the negative values, while $A_{\text{LeakyReLU}}$ preserves the negative values. A_{softmax} indicates the attention map is computed following VSA. The above four methods adopt the same Spikformer framework and apply weights to the spike-form V .

As shown in Table 1, our A_{SSA} outperforms A_I and $A_{\text{LeakyReLU}}$, demonstrating the advantage of computing attention map using \mathcal{SN} . We speculate that A_{SSA} surpasses A_{ReLU} because A_{SSA} exhibits stronger non-linearity in self-attention. Through comparative analysis with A_{softmax} , our proposed model, A_{SSA} , exhibits competitive performance and even outperforms A_{softmax} in terms of CIFAR10DVS and CIFAR10 datasets. The superiority of SSA over VSA in handling spike sequences (X and V) with restricted information can be ascribed to its inherent adaptability. Additionally, the computational complexity and theoretical energy consumption associated with the calculation of Q, K, V by A_{SSA} are considerably reduced compared to alternative methods.

SSA is specifically tailored for the purpose of modeling spike sequences. By representing Q, K , and V in spike form, the matrix dot-product calculation is simplified to logical AND and summation operations. For instance, considering

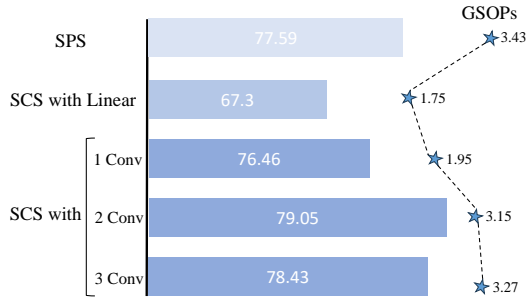


Fig. 4: Redesign of patch-splitting module. SPS represents the ImageNet accuracy achieved using Spikformer with SPS. When we remove max-polling, the accuracy of SCS with Linear layers sees a significant drop (the second row), whereas SCS with Convolutional layers performed better and reached its peak with the two-layer convolution configuration. All models have approximately the same number of parameters. GSOPs represents the theoretical synaptic operations.

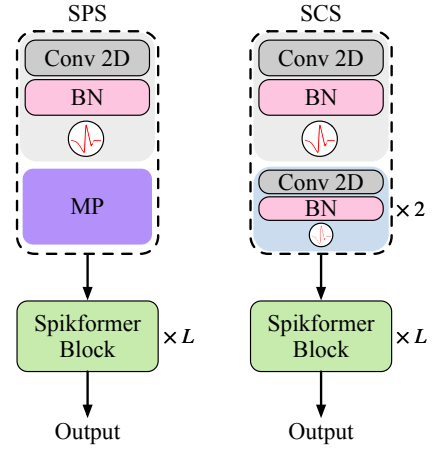
a row of Query q and a column of Key k , the calculation $\sum_{i=1}^d q_i k_i = \sum_{q_i=1} k_i$ illustrates this transformation. Furthermore, as depicted in Table 1, our proposed model, SSA, exhibits reduced computational burden and energy consumption attributed to the sparsity of spike-form Q , K , and V (as illustrated in Fig. 2) and the simplified calculations. Moreover, the order of computation between Q , K , and V is interchangeable: either performing QK^T first followed by V , or conducting $K^T V$ first followed by Q . In scenarios where the sequence length N exceeds the dimensionality d of a single head, the latter computation order incurs lower computational complexity ($O(Nd^2)$) compared to the former ($O(N^2d)$). SSA preserves both the biological plausibility and computational efficiency properties consistently throughout the entire calculation process.

4 SPIKFORMER V2

In this section, we propose a Spiking Convolutional Stem (SCS) to replace the original SPS, aiming to alleviate the issues of blurry spike block features and the inability to perform mask pre-training. Additionally, Self-Supervised Learning for Spikformer is explored to further enhance the performance of SNNs on ImageNet. With the introduction of the enhanced SCS and Self-Supervised Learning, an updated version of the model that is more focused on larger-scale models is obtained, referred to as Spikformer V2.

4.1 Spiking Convolutional Stem (SCS)

Prior research [32] identified the importance of the SPS module in Spikformer, which integrates convolution and progressive down-sampling. Despite performing well on small datasets, the model performance on ImageNet is not competitive. Additionally, the Spikformer using the SPS module cannot gain performance benefits from self-supervised pre-training. As indicated in Table 3, the result of the Spikformer employing SPS after SSL and fine-tuning is lower than that of supervised training (75.23% VS. 78.23%). We attribute this phenomenon to two main reasons: 1) The



(a) Spikformer with SPS (b) Spikformer with SCS

Fig. 5: Comparison between the Spiking Patch Splitting (SPS) and the Spiking Convolutional Stem (SCS). (a) In each block of the SPS module, the initial operation involves applying a 2D convolution with a kernel size of 3 and a stride of 1. This is followed by a max-pooling operation for downsampling by a factor of 2, which may lead to a potential loss of feature information. (b) In each block of the SCS module, the initial step involves downsampling using a 2D convolution with a kernel size of 2 and a stride of 2. Additionally, we augment each SCS block with a convolutional block structure similar to the MLP Block.

SPS comprises four ‘Conv-BN-LIF-MP’ blocks, with each block containing a max-pooling layer. Continuous max-pooling tends to result in a significant loss of information in spike-based features, and causes blurring of the features after SPS block mapping. Another study [29] has indicated that SPS can lead to erroneous gradient back-propagation. 2) In the earlier patch splitting module, stacking convolutions can greatly improve optimization stability and enhance peak performance [36]. Despite the presence of 1 convolutional layer in each SPS block, it is still insufficient to fully optimize the performance of the model. As illustrated in Fig. 4, upon removing max-pooling, the addition of linear layers within SCS leads to a sharp decline in performance, while adding convolutional layers (with a kernel size of 3, stride of 1, and padding of 1) results in a performance boost. To balance performance and efficiency, two additional convolutional layers are introduced within each SCS block.

Inspired by the aforementioned insights, we propose a redesigned patch splitting module for Spikformer, referred to as the Spiking Convolutional Stem (SCS) Module, which is shown in Fig. 5. This module differs from the SPS module in two main aspects. Firstly, instead of utilizing max-pooling for downsampling, SCS employs standard 2D convolution [4], thereby avoiding information loss in feature representation. Secondly, we introduce an increased number of convolutional layers, where two consecutive layers form a group. Existing studies [76] have suggested that the MLP blocks play a crucial role in learning shallow-level features. Therefore, we structure these two convolutional layers to resemble MLP blocks, enabling SCS with the combined advantages of both convolutional layers and MLP blocks. Specifically, similar

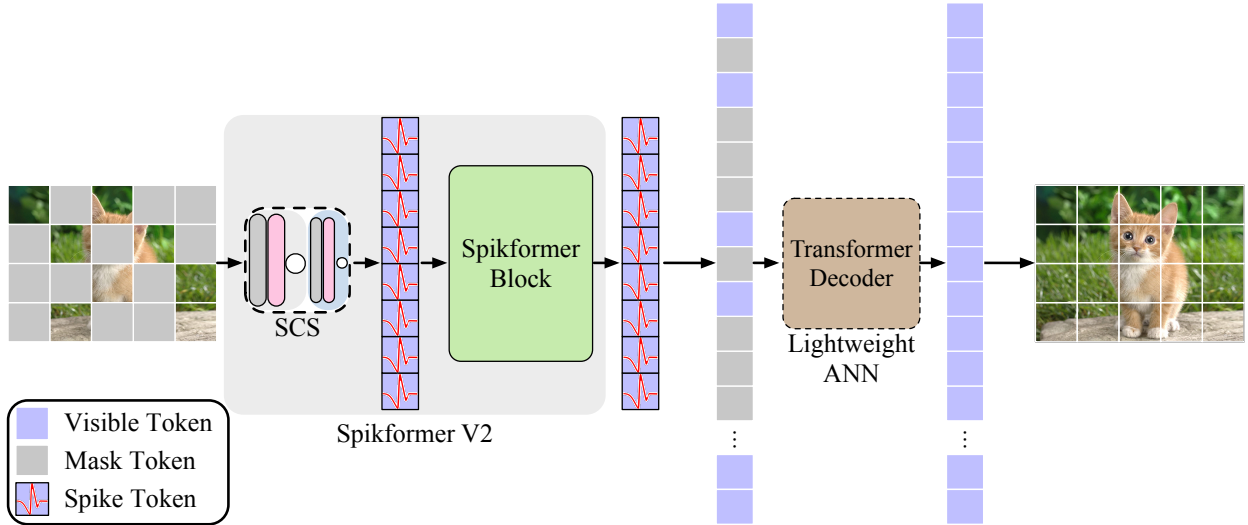


Fig. 6: Self-supervised pre-training on Spikformer V2 using the Mask Auto-Encoder framework. The SCS spike tokens are randomly masked using a high mask ratio. Spikformer V2 performs feature modeling on visible image patches and outputs spike tokens, while Transformer reconstructs the images using floating-point mask tokens and visible tokens. To prevent information leakage from masked patches, we adopt sparse convolution and sparse batch normalization in SCS, following the approach used in MC-MAE [74] and SparK [75]. The Transformer is a lightweight network (3.41M) that is discarded after pre-training.

to the MLP Block, the first convolutional layer expands the feature dimension by a ratio, while the second layer maps it back to the original dimension. This design does not significantly increase the number of parameters since the feature dimension in this module is typically small, such as 64, 128. Moreover, we argue that, while maintaining parameter efficiency, maximizing the depth of the network and the number of convolution layers is desirable. By default, we utilize a patch size of 16 to process ImageNet with a resolution of 224. This implies that the SCS requires the stacking of four blocks. Specifically, given an image with dimensions $H \times W$, the four SCS blocks yield spatial resolutions of $\frac{H}{2} \times \frac{W}{2}$, $\frac{H}{4} \times \frac{W}{4}$, $\frac{H}{8} \times \frac{W}{8}$, and $\frac{H}{16} \times \frac{W}{16}$, respectively.

Inspired by ANNs [22], [76], the Spikformer V2 with SCS adopts a deeper and narrower design compared to its previous version with SPS. Specifically, it has more convolutional layers in the SCS module, resulting in a deeper overall network. With a similar number of parameters, the Spikformer V2-8-384 model has lower dimensions compared to the Spikformer-8-512 model, indicating a narrower network design. Table 2 demonstrates that, under comparable parameter settings, incorporating the SCS into Spikformer V2 leads to improved performance in supervised training compared to the original Spikformer.

4.2 Self-supervised Pre-training

Despite the performance improvement achieved by the Spikformer V2, we observe a certain degree of performance degradation when further scaling up and deepening the Spikformer V2, as shown in Fig. 7. This phenomenon aligns with what is observed in ANNs [4], [21], mainly attributed to the instability and overfitting during the training of large models. Concretely, large models such as ViT-Large and ViT-Huge exhibited unstable training and lower performance. Unlike

ANN-Transformers, where the performance saturation or degradation typically occurs above 24 layers [77], the issue becomes apparent in Spikformer V2 with 12 or more layers. The Mask Auto-encoding mechanism [5] in Self-Supervised Learning can effectively train deep and large models and additionally improve model performance.

In addition to structural improvements in Spikformer V2, we also explore Self-Supervised Learning (SSL) for SNN-Transformers to further enlarge the model and enhance its representational capacity. SSL has gained significant popularity in ANNs and is considered a fundamental methodology for studying multimodal learning [78], and large-scale models [79]. However, the effectiveness of SSL in SNNs has not been extensively investigated. It is essential to conduct corresponding research to validate the feasibility and efficacy of SSL in SNNs. As a prevalent learning approach observed in the brain [80], [81], Self-Supervised Learning can also enhance the representational capacity of neural networks. Among various Self-Supervised Learning, the Mask Auto-encoding is most suitable for Spikformer V2. It adopts a decoupled encoder-decoder architecture to enhance the representation ability of the encoder by reconstructing the masked images using the decoder.

We devise an asymmetric SNN-ANN heterogeneous encoder-decoder architecture, as illustrated in Fig. 6. The SNN-encoder exclusively processes the partially observed signal (without mask tokens), while a lightweight ANN-decoder reconstructs the complete signal using the latent representation and mask tokens. The framework introduces a novel approach that couples SNN and ANN, utilizing the powerful modeling capabilities of ANN to enhance the representational capacity of SNN. This represents the third method, following the techniques of ANN2SNN and ANN distillation into SNN, for enhancing SNN through the utilization of ANN.

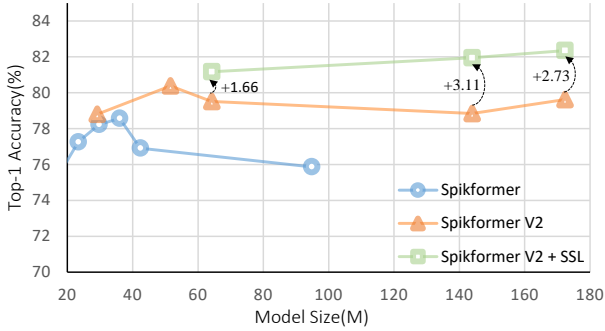


Fig. 7: Performance curve with expanded model parameters. The blue circles represent the performance changes of the previous version of Spikformer with increasing network depth and model parameters during supervised training. The orange triangles represent Spikformer V2. These curves indicate that, under supervised learning, the performance of the model tends to decline as the depth and number of parameters increase. In contrast, the green squares represent Spikformer V2 with mask autoencoder pre-training, demonstrating stable performance gains on larger and deeper models.

Masking. Following MAE [5], we employ a random sampling strategy for the masking operation on the N patches with a size of $\frac{H}{16} \times \frac{W}{16}$ after SCS splitting. Specifically, we select a subset N_v of patches following a uniform distribution and remove (i.e., mask) the remaining patches N_m . Consequently, a $\frac{H}{16} \times \frac{W}{16}$ mask M is generated, where a value of 1 represents the preservation of the corresponding patch in the feature map, while a value of 0 indicates its removal. Despite the fact that the Spikformer V2 patches are in the form of spikes, we observed that a high masking rate (e.g., 75%) remains applicable. This suggests that even in sparse spike signals, redundant information exists, providing insights for the future exploration of efficient SNN training.

Regarding the SCS, we adopt a similar methodology as MC-MAE [74] to obtain the corresponding masks. Specifically, we upsample the generated mask M by factors of 8, 4, and 2, respectively, to serve as masks for the first, second, and third SCS blocks. The fourth SCS block can directly utilize the mask M .

Spikformer V2 encoder. The encoder utilized the Spikformer V2 with SCS, as described in Sec. 4.1. During the pre-training process, the encoder exclusively processes the visible patches. Apart from utilizing a high masking rate, we further enhance the efficiency of pre-training in Spikformer by setting the time step to 1. This ensures that the reconstruction during pre-training is sufficiently challenging, which is beneficial for the downstream fine-tuning task [5], [74], [75].

Transformer decoder. We employ a lightweight ANN-Transformer as the decoder, which has better image reconstruction ability than the SNN-decoder. The decoder is discarded after pre-training; it does not affect the fact that our Spikformer V2 is a pure SNN. As shown in Fig. 6, the decoder receives a complete set of tokens, comprising encoded visible patches and mask tokens, as input. The mask tokens are replicated from a shared learnable vector, serving as an indicator for the presence of a missing patch that needs

to be predicted. Positional embeddings are incorporated into all tokens within the complete set, ensuring that mask tokens possess information about their spatial location in the image.

Training Cost. The motivation is to explore Self-Supervised Learning in SNNs and to consistently enhance the performance of large-scale Spikformer V2. Additionally, we have observed its advantage in reducing training costs. We compare the training cost between supervised training and fine-tuning after pre-training and find it can achieve training acceleration while maintaining stable training and performance improvements, which are shown in Table 3. As the model parameter size increases, the training acceleration ratio of SSL compared to direct supervised training becomes more prominent. It is worth noting that while in ANNs, pre-training typically involves more than 800 epochs, we find that even with fewer pre-training epochs in SNNs, we can still achieve good fine-tuning results on ImageNet. And the finetune performance increases with the increase of pre-training epochs, as shown in Table 7.

5 EXPERIMENTS

In this section, we begin by evaluating the performance of the proposed Spikformer and Spikformer V2 on the large-scale image classification dataset, ImageNet [19]. We further conduct an analysis of the structural enhancements incorporated in Spikformer V2, as well as the performance improvements achieved through SSL pre-training. Additionally, we present the performance of Spikformer on small-scale static datasets. Furthermore, we evaluate the classification performance of Spikformer on popular neuromorphic datasets. Finally, we include ablation experiments and partial visualizations as the concluding part of this section.

5.1 Supervised learning experiments on ImageNet

5.1.1 Experimental Settings.

ImageNet-1K [19] is a widely used static image dataset for image classification. It consists of 1,000 categories and contains approximately 1.28 million training images and 50,000 test images. The images are resized to a default size of 224×224 for both training and evaluation. We employ the AdamW optimizer [90] for training, utilizing a cosine decay learning rate scheduler for 300 epochs. Additionally, we incorporate 10 epochs of linear warm-up. Similar to the supervised training strategy in MAE [5], we employed a per-iteration learning rate update policy. We adopt a batch size of 512, distributed across 8 Nvidia V100 GPUs. We set the initial learning rate to 0.0005 and apply a weight decay of 0.05. In contrast to ANN-Transformers [4], [22], we do not employ drop path in our approach, as we have found that it does not enhance performance. Moreover, following DeiT [21], [25], data augmentation techniques including RandAugment [91], random erasing [92], and stochastic depth [93] are employed for data augmentation in our approach. Nevertheless, we refrain from incorporating Mixup [94] and Cutmix [95] for data augmentation in our approach. This decision stems from the recognition that the transformation of static RGB images into spiking event data already poses significant challenges for the classification task. The inclusion of Mixup and Cutmix techniques on spiking data would introduce

TABLE 2: Evaluation on ImageNet. Param refers to the number of parameters. Power denotes the average theoretical energy consumption during image prediction on the ImageNet test set. Spikformer- L - D is a Spikformer model with L Spikformer encoder blocks and D feature embedding dimensions. OPs refers to SOPs in SNNs and FLOPs in ANNs.

Category	Methods	Architecture	Param (M)	OPs (G)	Power (mJ)	Time Step	Acc
ANN-to-SNN	Hybrid training [82]	ResNet-34	21.79	-	-	250	61.48
	Spiking ResNet [31]	ResNet-34	21.79	65.28	59.295	350	71.61
		ResNet-50	25.56	78.29	70.934	350	72.75
	QCFS [83]	VGG-16	138.42	-	-	64	72.85
	Fast-SNN [84]	VGG-16	138.42	-	44.850	7	72.95
	COS [85]	ResNet-34	21.79	-	8.070	8	74.17
ANN	T2T-ViT [22]	T2T-ViT-24	64.10	13.80	63.516	1	82.30
	PVT [24]	PVT-Large	61.40	9.80	38.340	1	81.70
	Swin Transformer [25]	SWIN-Base	88.00	15.40	70.880	1	83.50
		ViT-Base	86.60	17.60	95.310	1	82.30
	MAE [5]	ViT-Large	307.00	-	-	1	82.60
Directly Learning	TET [86]	Spiking-ResNet-34	21.79	-	-	6	64.79
	STBP-tdBN [28]	SEW-ResNet-34	21.79	-	-	4	68.00
		Spiking-ResNet-34	21.79	6.50	6.393	6	63.72
	SEW ResNet [14]	SEW-ResNet-34	21.79	3.88	4.035	4	67.04
		SEW-ResNet-50	25.56	4.83	4.890	4	67.78
		SEW-ResNet-101	44.55	9.30	8.913	4	68.76
		SEW-ResNet-152	60.19	13.72	12.891	4	69.26
	Attention-SNN [87]	ResNet-104	78.37	-	7.300	4	77.08
	Spike-driven Transformer [88]	Spiking Transformer-8-768	66.34	-	6.090	4	77.07
	Spikingformer [89]	Spiking Transformer-8-768	66.34	12.54	13.680	4	75.85
CML [29]	Spiking Transformer-8-768	66.34	-	-	4	77.64	
Directly Learning	Spikformer	Spikformer-8-384	16.81	6.63	5.967	4	75.24
		Spikformer-6-512	23.37	8.21	7.389	4	77.26
		Spikformer-8-512	29.68	10.95	9.855	4	78.23
		Spikformer-10-512	36.01	13.67	12.303	4	78.57
		Spikformer-8-768	66.34	22.22	19.998	4	79.55
Directly Learning	Spikformer V2	Spikformer V2-8-384	29.11	1.92	1.728	1	75.42
		Spikformer V2-8-512	29.11	5.21	4.689	4	78.80
		Spikformer V2-8-512	51.55	3.15	2.835	1	79.05
		Spikformer V2-8-512	51.55	10.40	9.360	4	80.38

additional complexities to the classification process on large-scale datasets and potentially impede convergence.

5.1.2 Results.

The supervised learning results of Spikformer and Spikformer V2 are presented in Table 2. The experimental results demonstrate the superior performance of our proposed Spikformer and Spikformer V2 compared to previous state-of-the-art models, including both the ANN2SNN and direct training methods, across various model sizes. Specifically, considering the Spikformer V2-8-512 model with 51.55 million parameters as a representative example, we observe that even when tested on a resolution of 224 with 4 time steps, it achieves an impressive top-1 accuracy of 80.38% on the ImageNet. Compared to the state-of-the-art Attention-SNN [87] model, our model achieves a 3.3% increase in classification accuracy while having half the number of parameters. Note that the A-SNN model is trained using images of resolution 288. To the best of our knowledge, this is the first time that an SNN model has achieved an accuracy of over 80% on ImageNet, and it is accomplished using the Spikformer V2-base model with low simulation latency (4 steps). This breakthrough challenges the common perception of low performance in SNNs and demonstrates the potential of SNNs. While achieving high accuracy, Spikformer V2 also demonstrates competitive theoretical energy efficiency. In comparison

to the previous version of Spikformer, the Spikformer V2 achieves certain performance improvements (approximately 0.5%) while maintaining a similar number of parameters. For example, 29.11M Spikformer V2-8-384 achieves a 0.57% higher performance compared to 29.68M Spikformer-8-512, while energy consumption is only 0.48 times that of the other. This demonstrates the effectiveness of SCS and the narrow and deep design. The Spikformer V2-8-512, which has fewer parameter (51.55M VS. 66.34M), achieves higher classification performance than Spikformer V2-8-768 (80.38% VS. 79.55%). Specifically, compared to ANNs, Spikformer V2-8-512 achieves similar accuracy (80.38%) with only one-tenth of the energy consumption.

Spikformer V2 also demonstrates excellent performance in a pure binary spiking residual connection, as shown in Table 6. We replace the ADD operator in the original network with the IAND operator from SEW ResNet [14], transforming the entire network into one that utilizes pure binary activation for inter-layer information propagation. Even in this binary spiking setting, Spikformer V2-8-512 still achieves a performance of 76.12%.

Although there is still a performance gap between Spikformer and Spikformer V2 compared to ANN-Transformers, as shown in Table 2, it is not doubtful that our work has taken the first step in exploring high-performance SNN models. We firmly believe that future SNN models can achieve both

TABLE 3: Comparisons between directly supervised learning and Self-Supervised Learning + finetune. Speedup ratio refers to the supervised learning training time of the Spikformer V2 model with the same parameter divided by the SSL training time.

Learning Method	Model	Param (M)	Training Epoch	Training Time (h)	Speedup	Time Step	OPs (G)	Power (mj)	Acc.
Learning on ANN	ViT-Base	86.60	300	-	-	1	17.60	95.310	82.30
	ViT-Large	307.00	300	-	-	1	-	-	82.60
	T2T-ViT-24	64.10	300	-	-	1	13.80	63.516	82.30
	PVT-Large	61.40	300	-	-	1	9.80	38.340	81.70
	SWIN-Base	88.00	300	-	-	1	15.40	70.880	83.50
Supervised Learning	Spikformer V1-8-512	29.69	300	-	-	4	10.95	11.304	78.23
Pre-training + Finetune	Spikformer V1-8-512	29.69	200 + 150	-	-	4	-	-	75.23
Supervised Learning	Spikformer V2-8-512	51.55	300	85	1×	1	3.15	2.835	79.05
	-	-	-	102	-	4	10.40	9.360	80.38
	Spikformer V2-12-512	64.18	300	100	1×	1	4.15	3.735	78.65
	Spikformer V2-12-768	143.89	300	155	1×	1	6.35	5.715	76.61
	Spikformer V2-16-768	172.28	300	240	1×	1	7.64	6.876	77.43
Pre-training + Finetune	Spikformer V2-12-512	64.18	200+150	96.7	1.03×	1	4.01	3.609	79.64
	-	-	-	-	-	4	16.31	14.680	81.17
	Spikformer V2-12-768	143.89	200+150	147.5	1.05×	1	6.40	5.760	80.49
	-	-	-	-	-	4	19.97	17.970	81.94
	Spikformer V2-16-768	172.70	200+150	196.7	1.22×	1	7.48	6.732	81.10
-	-	-	-	-	4	28.42	25.578	82.35	

high performance and low energy consumption.

5.2 Self-Supervised Learning on ImageNet.

In order to further enhance the performance of Spikformer V2 and address the issue of limited scalability of its model size, we introduce self-supervised pre-training using masked image modeling into Spikformer V2.

5.2.1 Experimental Settings.

We conducted SSL pre-training on the ImageNet training set. The mask ratio is fixed at 75% based on the original MAE [5]. The ANN-Transformer decoder consists of 4 transformer layers with 256 feature dimensions and 4 attention heads. During pre-training, we employ a cosine learning rate schedule with 200 epochs, where the first 20 epochs are dedicated to warm-up. The AdamW optimizer is adopted with a base learning rate of 1×10^{-3} , a weight decay of 0.05, and a batch size of 1024. To augment the data during pre-training, we employed random cropping. The reconstruction target is the normalized input image. Although the reconstruction results of Spikformer as an encoder are inferior to that of MAE in ANN, which is shown in Fig. 8, fine-tuning performance after pre-training reveals that the RGB image reconstruction task is also applicable to Spikformer V2.

After the pre-training, we perform supervised fine-tuning on the ImageNet training set using the cosine learning rate schedule for 150 epochs. We utilize a per-iteration-update cosine decay learning rate strategy with a base learning rate of 1×10^{-3} . We employ a layer-wise learning rate decay strategy following MAE, where the learning rate of each upper layer in the network is set to 0.7 times the learning rate of the subsequent layer. To reduce training overhead, we finetune the model using a single-time step model to obtain results on multiple time steps (e.g., 2, 4, 6). The base learning rate is set to 1×10^{-5} , and the fine-tuning is performed for 20 epochs.

5.2.2 Results.

As shown in Table 3, after pre-training, the performance of Spikformer V1 actually decreases, which could be attributed to the presence of max-pooling in the SPS module of Spikformer V1. This max-pooling operation leads to information loss during feature extraction and is not suitable for complex image reconstruction tasks during pre-training.

The performance of Spikformer V2 is significantly improved through self-supervised pre-training. Moreover, it demonstrates stable performance improvements, particularly in large models. Specifically, the Spikformer V2-12-768 model achieves an accuracy of 80.49% using only a single time step. Using one time step, the Spikformer V2-16-768 model achieves an accuracy of 81.10%, which is 3.67% higher than the result obtained from supervised directly training (77.43%). Although the accuracy is steadily improved, the energy consumption of the model after SSL does not increase significantly, but is similar to that of the supervised training model. The utilization of SSL accelerates network training, with the acceleration ratio increasing as the network parameters grow in size. The 172M Spikformer V2-16-768 not only achieves performance enhancement but also experiences a training acceleration of 1.22 times.

5.3 Small datasets classification

We evaluate the performance of Spikformer on small-scale datasets, including CIFAR, DVS-Gesture, and CIFAR10DVS. As Spikformer V2 is primarily designed for ImageNet, its performance on these smaller datasets was comparatively lower than that of Spikformer V1. Because SPS is specifically designed for small datasets and can achieve better performance than SCS.

5.3.1 CIFAR.

The CIFAR dataset consists of 50,000 training images and 10,000 test images, all of which have a resolution of 32×32 .

TABLE 4: Comparison of the performance between Spikformer and existing approaches on CIFAR10/100. * denotes self-implementation results by [86]. Note that Hybrid training [82] adopts ResNet-20 for CIFAR10 and VGG-11 for CIFAR100.

Methods	Param (M)	Time Step	CIFAR10 Acc	CIFAR100 Acc
Hybrid training [82]	9.27	125	92.22	67.87
Diet-SNN [96]	0.27	10/5	92.54	64.07
STBP [54]	17.54	12	89.83	-
STBP NeuNorm [97]	17.54	12	90.53	-
TSSL-BP [98]	17.54	5	91.41	-
STBP-tdBN [28]	12.63	4	92.92	70.86
TET [86]	12.63	4	94.44	74.47
ResNet-19*	12.63	1	94.97	75.35
Transformer-4-384	9.32	1	96.73	81.02
Spikformer-4-256	4.15	4	93.94	75.96
Spikformer-2-384	5.76	4	94.80	76.95
Spikformer-4-384	9.32	4	95.19	77.86
Spikformer-4-384 400E	9.32	4	95.51	78.21

For our experiments, we use a batch size of 128. We employ a four-block SPS architecture, where the first two blocks do not include the max-pooling layer. The image is divided into $64 \times 4 \times 4$ patches. Table 4 presents the accuracy of our method (Spikformer) in comparison to other models on the CIFAR dataset. As depicted in Table 4, our Spikformer-4-384 achieves an accuracy of 95.19% on the CIFAR10 dataset, surpassing the performance of TET (94.44%) and ResNet-19 ANN (94.97%). Notably, the performance continues to improve with increasing dimensions and blocks. In particular, Spikformer-4-384 demonstrates a 1.25% improvement compared to Spikformer-4-256 and a 0.39% improvement compared to Spikformer-2-384. Moreover, we observe that increasing the number of training epochs to 400 leads to performance enhancement (Spikformer-4-384 400E achieves a 0.32% and 0.35% improvement compared to Spikformer-4-384 on CIFAR10 and CIFAR100, respectively). Notably, the performance gain of Spikformer is even more significant on complex datasets like CIFAR100. Specifically, Spikformer-4-384 (77.86%, 9.32M) achieves a substantial improvement of 2.51% compared to the ResNet-19 ANN (75.35%, 12.63M) model. However, the performance of ANN-Transformer still surpasses that of Spikformer, achieving a 1.22% and 2.81% higher accuracy than the latter on CIFAR10 and CIFAR100, respectively.

5.3.2 Neuromorphic datasets classification

The DVS128 Gesture dataset is a collection of gesture recognition data, consisting of 11 hand gesture categories performed by 29 individuals under 3 illumination conditions. Similarly, CIFAR10-DVS is a neuromorphic dataset derived from the CIFAR10 static image dataset. It involves shifting image samples to capture their spike events with a DVS camera. CIFAR10-DVS consists of 9,000 training samples and 1,000 test samples.

For the aforementioned datasets with an image size of 128×128 , we employ a four-block SPS architecture. The patch embedding dimension is set to 256, and the patch size is 16×16 . We utilize a shallow Spikformer model, which consists of 2 transformer encoder blocks. The SSA module includes 8

TABLE 5: Comparison of the performance with state-of-the-art (SOTA) methods on two neuromorphic datasets. Bold font means the best; * denotes with Data Augmentation.

Method	Spikes	CIFAR10-DVS		DVS128	
		T Step	Acc	T Step	Acc
LIAF-Net [100]	✗	10	70.4	60	97.6
TA-SNN [16]	✗	10	72.0	60	98.6
Rollout [101]	✓	48	66.8	240	97.2
DECOLLE [102]	✓	-	-	500	95.5
tdBN [28]	✓	10	67.8	40	96.9
PLIF [17]	✓	20	74.8	20	97.6
SEW-ResNet [14]	✓	16	74.4	16	97.9
Dspike [103]	✓	10	75.4*	-	-
SALT [104]	✓	20	67.1	-	-
DSR [59]	✓	10	77.3*	-	-
Spikformer	✓	10	78.9*	10	96.9
	✓	16	80.9*	16	98.3

heads for DVS128 Gesture and 16 heads for CIFAR10-DVS. A time step of 10 or 16 is utilized. The training process involves 200 epochs for DVS128 Gesture and 106 epochs for CIFAR10-DVS. The AdamW optimizer is utilized, and the batch size is set to 16. The learning rate starts at 0.001 and is reduced using a cosine decay schedule. For CIFAR10-DVS, we apply data augmentation techniques as described in [99]. Additionally, we employ a learnable parameter to control the scaling factor of the $QK^T V$ computation.

The classification performance of Spikformer and the compared state-of-the-art models on neuromorphic datasets is presented in Table 5. It can be observed that our model achieves impressive performance on both datasets while utilizing a compact model size of 2.59M parameters. Specifically, on the DVS128 Gesture dataset, we achieve an accuracy of 98.2% using 16 time steps, outperforming the SEW-ResNet model (97.9%). Furthermore, our results are competitive with the TA-SNN model (98.6%, 60 time steps) [16], which employs floating-point spikes in the forward propagation process.

On the CIFAR10-DVS dataset, our Spikformer model outperforms the state-of-the-art methods in terms of accuracy. Specifically, we achieve a 1.6% and 3.6% higher accuracy compared to the DSR, which utilizes binary spikes and employs 10 and 16 time steps, respectively (DSR achieves 77.3% accuracy). It is worth noting that we do not compare our results with the TET in the table since TET is not an architecture-based method but a loss-based method. TET achieves 83.2% accuracy by using long epochs (300) and a larger model size of 9.27M parameters using VGG-SNN.

5.4 Ablation Studies

5.4.1 Time Step

The accuracy results for different simulation time steps of the spiking neuron are presented in Table 6. When the time step is set to 1, our method exhibits a 1.87% decrease in accuracy compared to the network with a time step of 4 on CIFAR10. However, even with only 1 time step, Spikformer-8-512 and Spikformer V2-8-512 achieve a respectable accuracy of 76.01% and 79.05%, respectively. These findings demonstrate the robustness of Spikformer under low latency conditions, where fewer time steps are utilized.

TABLE 6: Ablation study results on SSA, and time step.

Datasets	Models	Time Step	Top1-Acc (%)	
CIFAR10/100	Spikformer-4-384 _w SSA	1	93.51/74.36	
		2	93.59/76.28	
		4	95.19/77.86	
		6	95.34/78.61	
	Spikformer-4-384 _w VSA	4	94.97/77.92	
		Spikformer-4-384 _w VSA V _F	4	95.17/78.37
ImageNet	Spikformer-8-512 _w I	4	✗	
		4	✗	
		4	✗	
		4	77.92	
		4	79.03	
	Spikformer V2-8-512 _w SSA	1	76.01	
		2	77.18	
		4	78.23	
		6	78.57	
		1	79.05	
Spikformer V2-8-512-IAND	2	79.20		
	4	80.38		
	6	80.73		
1	76.12			

TABLE 7: Ablation experiments of SSL. We use Spikformer V2-12-512 as the encoder on ImageNet classification under various mask ratios, pre-training epoch and finetuning epoch configurations.

Mask Ratio	Pretrain Epoch	Finetune Epoch	Top-1 Acc.
75%	200	150	79.64
75%	400	150	79.71
75%	800	150	79.90
75%	200	200	79.93
60%	200	150	79.40
50%	200	150	79.73

5.4.2 Setting in SSL

Mask ratio, pre-training epochs, and finetuning epochs are crucial configuration parameters of SSL. We conduct ablation experiments on these three parameters separately, as depicted in Table 7. Extending the number of pre-training and finetuning epochs has shown potential for yielding performance improvements to a certain extent. Moreover, altering the mask ratio to a certain degree also influences performance. In consideration of a balanced trade-off between training costs and performance, a mask ratio of 75% has been adopted. The implication of higher mask ratios suggests a similarity to the floating-point feature [5], indicating the presence of significant spatial redundancy within the spiking feature as well.

5.4.3 Visualization of Image Reconstruction

We apply masking to the images and employ the SNN-ANN encoder-decoder framework for reconstruction, as depicted in Fig. 8. The reconstruction demonstrates favorable outcomes, indicating the effectiveness of pre-training. However, the reconstruction performance is comparatively inferior to that of ANN-MAE. This discrepancy can be attributed to the fact that the task of reconstruction poses challenges for the SNN encoder, which relies on utilizing spiking features for inter-layer propagation. Furthermore, in contrast to the original MAE employing an 8-layer 384-dimensional decoder, we utilize a lightweight 4-layer 256-dimensional

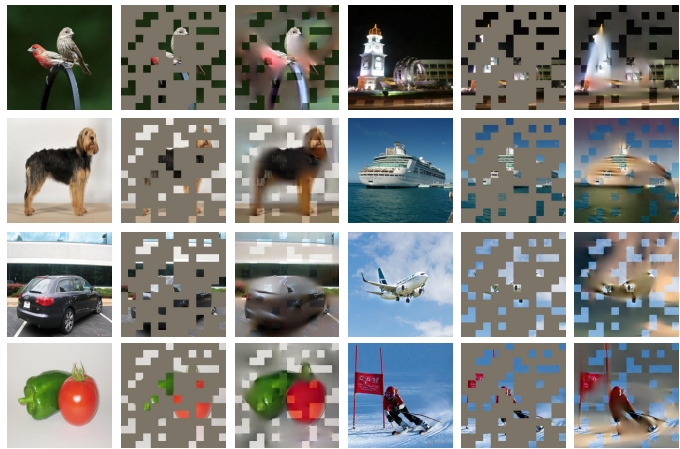


Fig. 8: Mask and Reconstruction Examples. For each triplet, we present the original image (left), masked image (middle), and reconstructed image (right). The mask ratio is set at 75%, and the encoder employed is Spikformer V2-12-512.

ANN decoder. This choice also contributes to the relatively inferior reconstruction performance compared to ANN-MAE.

6 CONCLUSIONS AND FUTURE WORK

In this paper, we propose the Transformer framework for SNNs, called Spiking Transformer (Spikformer), which achieves state-of-the-art performance in SNNs by leveraging the spiking self-attention mechanism. Besides, to address the issue of low performance of SNNs, including Spikformer, on ImageNet, we further optimized the Spikformer’s architecture and introduced self-supervised pre-training, leading to the proposal of Spikformer V2. Our method achieves a significant breakthrough in the field of SNNs, surpassing the high-accuracy bottleneck on ImageNet (80%). We hope that the strong performance of Spikformer V2 will encourage further research on better SNN-Transformer and SNN-Self-Supervised Learning.

Despite these contributions, certain limitations still exist. Concretely, experiments on other visual downstream tasks, such as object detection and semantic segmentation, have not been conducted due to the lack of widely adopted detection and segmentation frameworks for direct training of SNNs. In the future, we will focus on exploring the performance of Spiking Transformers on various visual tasks and aim to establish a comprehensive visual algorithm system for SNN-Transformers.

REFERENCES

- [1] J. Devlin, M.-W. Chang, K. Lee, and K. Toutanova, “Bert: Pre-training of deep bidirectional transformers for language understanding,” *arXiv preprint arXiv:1810.04805*, 2018.
- [2] T. Brown, B. Mann, N. Ryder, M. Subbiah, J. D. Kaplan, P. Dhariwal, A. Neelakantan, P. Shyam, G. Sastry, A. Askell *et al.*, “Language models are few-shot learners,” *Advances in neural information processing systems*, vol. 33, pp. 1877–1901, 2020.
- [3] H. Touvron, T. Lavril, G. Izacard, X. Martinet, M.-A. Lachaux, T. Lacroix, B. Rozière, N. Goyal, E. Hambro, F. Azhar *et al.*, “Llama: Open and efficient foundation language models,” *arXiv preprint arXiv:2302.13971*, 2023.

- [4] A. Dosovitskiy, L. Beyer, A. Kolesnikov, D. Weissenborn, X. Zhai, T. Unterthiner, M. Dehghani, M. Minderer, G. Heigold, S. Gelly *et al.*, “An image is worth 16x16 words: Transformers for image recognition at scale,” in *International Conference on Learning Representations (ICLR)*, 2020.
- [5] K. He, X. Chen, S. Xie, Y. Li, P. Dollár, and R. Girshick, “Masked autoencoders are scalable vision learners,” in *Proceedings of the IEEE/CVF Conference on Computer Vision and Pattern Recognition*, 2022, pp. 16 000–16 009.
- [6] A. Kirillov, E. Mintun, N. Ravi, H. Mao, C. Rolland, L. Gustafson, T. Xiao, S. Whitehead, A. C. Berg, W.-Y. Lo *et al.*, “Segment anything,” *arXiv preprint arXiv:2304.02643*, 2023.
- [7] A. Brohan, N. Brown, J. Carbajal, Y. Chebotar, J. Dabis, C. Finn, K. Gopalakrishnan, K. Hausman, A. Herzog, J. Hsu *et al.*, “Rt-1: Robotics transformer for real-world control at scale,” *arXiv preprint arXiv:2212.06817*, 2022.
- [8] W. Maass, “Networks of spiking neurons: the third generation of neural network models,” *Neural networks*, vol. 10, no. 9, pp. 1659–1671, 1997.
- [9] P. A. Merolla, J. V. Arthur, R. Alvarez-Icaza, A. S. Cassidy, J. Sawada, F. Akopyan, B. L. Jackson, N. Imam, C. Guo, Y. Nakamura *et al.*, “A million spiking-neuron integrated circuit with a scalable communication network and interface,” *Science*, vol. 345, no. 6197, pp. 668–673, 2014.
- [10] M. Davies, N. Srinivasa, T.-H. Lin, G. Chinya, Y. Cao, S. H. Choday, G. Dimou, P. Joshi, N. Imam, S. Jain *et al.*, “Loihi: A neuromorphic manycore processor with on-chip learning,” *Ieee Micro*, vol. 38, no. 1, pp. 82–99, 2018.
- [11] J. Pei, L. Deng, S. Song, M. Zhao, Y. Zhang, S. Wu, G. Wang, Z. Zou, Z. Wu, W. He *et al.*, “Towards artificial general intelligence with hybrid tianji chip architecture,” *Nature*, vol. 572, no. 7767, pp. 106–111, 2019.
- [12] K. Roy, A. Jaiswal, and P. Panda, “Towards spike-based machine intelligence with neuromorphic computing,” *Nature*, vol. 575, no. 7784, pp. 607–617, 2019.
- [13] N. Perez-Nieves and D. Goodman, “Sparse spiking gradient descent,” in *Advances in Neural Information Processing Systems*, M. Ranzato, A. Beygelzimer, Y. Dauphin, P. Liang, and J. W. Vaughan, Eds., vol. 34. Curran Associates, Inc., 2021, pp. 11 795–11 808. [Online]. Available: https://proceedings.neurips.cc/paper_files/paper/2021/file/61f2585b0ebcf1f532c4d1ec9a7d51aa-Paper.pdf
- [14] W. Fang, Z. Yu, Y. Chen, T. Huang, T. Masquelier, and Y. Tian, “Deep Residual Learning in Spiking Neural Networks,” in *Proceedings of the International Conference on Neural Information Processing Systems (NeurIPS)*, vol. 34, 2021, pp. 21 056–21 069.
- [15] Y. Hu, Y. Wu, L. Deng, and G. Li, “Advancing residual learning towards powerful deep spiking neural networks,” *arXiv preprint arXiv:2112.08954*, 2021.
- [16] M. Yao, H. Gao, G. Zhao, D. Wang, Y. Lin, Z. Yang, and G. Li, “Temporal-wise attention spiking neural networks for event streams classification,” in *Proceedings of the IEEE/CVF International Conference on Computer Vision (ICCV)*, 2021, pp. 10 221–10 230.
- [17] W. Fang, Z. Yu, Y. Chen, T. Masquelier, T. Huang, and Y. Tian, “Incorporating learnable membrane time constant to enhance learning of spiking neural networks,” in *Proceedings of the IEEE/CVF International Conference on Computer Vision (ICCV)*, 2021, pp. 2661–2671.
- [18] X. Cheng, T. Zhang, S. Jia, and B. Xu, “Meta neurons improve spiking neural networks for efficient spatio-temporal learning,” *Neurocomputing*, vol. 531, pp. 217–225, 2023.
- [19] J. Deng, W. Dong, R. Socher, L.-J. Li, K. Li, and L. Fei-Fei, “Imagenet: A large-scale hierarchical image database,” in *Proceedings of the IEEE/CVF Conference on Computer Vision and Pattern Recognition (CVPR)*, 2009, pp. 248–255.
- [20] A. Dosovitskiy, L. Beyer, A. Kolesnikov, D. Weissenborn, X. Zhai, T. Unterthiner, M. Dehghani, M. Minderer, G. Heigold, S. Gelly, J. Uszkoreit, and N. Houlsby, “An image is worth 16x16 words: Transformers for image recognition at scale,” in *International Conference on Learning Representations*, 2021. [Online]. Available: <https://openreview.net/forum?id=YicbFdNTTy>
- [21] H. Touvron, M. Cord, M. Douze, F. Massa, A. Sablayrolles, and H. Jegou, “Training data-efficient image transformers & distillation through attention,” in *Proceedings of the International Conference on Machine Learning (ICML)*, vol. 139, 2021, pp. 10 347–10 357.
- [22] L. Yuan, Y. Chen, T. Wang, W. Yu, Y. Shi, Z.-H. Jiang, F. E. Tay, J. Feng, and S. Yan, “Tokens-to-token vit: Training vision transformers from scratch on imagenet,” in *Proceedings of the IEEE/CVF International Conference on Computer Vision (ICCV)*, 2021, pp. 558–567.
- [23] L. Yuan, Q. Hou, Z. Jiang, J. Feng, and S. Yan, “Volo: Vision outlooker for visual recognition,” *arXiv preprint arXiv:2106.13112*, 2021.
- [24] W. Wang, E. Xie, X. Li, D.-P. Fan, K. Song, D. Liang, T. Lu, P. Luo, and L. Shao, “Pyramid vision transformer: A versatile backbone for dense prediction without convolutions,” in *Proceedings of the IEEE/CVF International Conference on Computer Vision (ICCV)*, 2021, pp. 568–578.
- [25] Z. Liu, Y. Lin, Y. Cao, H. Hu, Y. Wei, Z. Zhang, S. Lin, and B. Guo, “Swin transformer: Hierarchical vision transformer using shifted windows,” in *Proceedings of the IEEE/CVF International Conference on Computer Vision (ICCV)*, 2021, pp. 10 012–10 022.
- [26] H. Chen, Y. Wang, T. Guo, C. Xu, Y. Deng, Z. Liu, S. Ma, C. Xu, C. Xu, and W. Gao, “Pre-trained image processing transformer,” in *Proceedings of the IEEE/CVF Conference on Computer Vision and Pattern Recognition (CVPR)*, 2021, pp. 12 299–12 310.
- [27] X. Chen, C. Liang, D. Huang, E. Real, K. Wang, Y. Liu, H. Pham, X. Dong, T. Luong, C.-J. Hsieh *et al.*, “Symbolic discovery of optimization algorithms,” *arXiv preprint arXiv:2302.06675*, 2023.
- [28] H. Zheng, Y. Wu, L. Deng, Y. Hu, and G. Li, “Going Deeper With Directly-Trained Larger Spiking Neural Networks,” in *Proceedings of the AAAI Conference on Artificial Intelligence (AAAI)*, 2021, pp. 11 062–11 070.
- [29] C. Zhou, H. Zhang, Z. Zhou, L. Yu, Z. Ma, H. Zhou, X. Fan, and Y. Tian, “Enhancing the performance of transformer-based spiking neural networks by improved downsampling with precise gradient backpropagation,” *arXiv preprint arXiv:2305.05954*, 2023.
- [30] S. Kundu, M. Pedram, and P. A. Beerel, “Hire-snn: Harnessing the inherent robustness of energy-efficient deep spiking neural networks by training with crafted input noise,” in *Proceedings of the IEEE/CVF International Conference on Computer Vision (ICCV)*, 2021, pp. 5209–5218.
- [31] Y. Hu, H. Tang, and G. Pan, “Spiking deep residual networks,” *IEEE Transactions on Neural Networks and Learning Systems*, pp. 1–6, 2021.
- [32] Z. Zhou, Y. Zhu, C. He, Y. Wang, S. YAN, Y. Tian, and L. Yuan, “Spikformer: When spiking neural network meets transformer,” in *The Eleventh International Conference on Learning Representations*, 2023. [Online]. Available: https://openreview.net/forum?id=frE4fUwz_h
- [33] A. Vaswani, N. Shazeer, N. Parmar, J. Uszkoreit, L. Jones, A. N. Gomez, Ł. Kaiser, and I. Polosukhin, “Attention is all you need,” in *Proceedings of the International Conference on Neural Information Processing Systems (NeurIPS)*, vol. 30, 2017.
- [34] Z. Qin, W. Sun, H. Deng, D. Li, Y. Wei, B. Lv, J. Yan, L. Kong, and Y. Zhong, “cosformer: Rethinking softmax in attention,” *arXiv preprint arXiv:2202.08791*, 2022.
- [35] K. Choromanski, V. Likhoshesterov, D. Dohan, X. Song, A. Gane, T. Sarlos, P. Hawkins, J. Davis, A. Mohiuddin, L. Kaiser *et al.*, “Rethinking attention with performers,” *arXiv preprint arXiv:2009.14794*, 2020.
- [36] T. Xiao, M. Singh, E. Mintun, T. Darrell, P. Dollár, and R. Girshick, “Early convolutions help transformers see better,” in *Proceedings of the International Conference on Neural Information Processing Systems (NeurIPS)*, vol. 34, 2021, pp. 30 392–30 400.
- [37] H. Bao, L. Dong, S. Piao, and F. Wei, “BEit: BERT pre-training of image transformers,” in *International Conference on Learning Representations*, 2022. [Online]. Available: <https://openreview.net/forum?id=p-BhZSz59o4>
- [38] C. Zhuang, S. Yan, A. Nayebi, M. Schrimpf, M. C. Frank, J. J. DiCarlo, and D. L. Yamins, “Unsupervised neural network models of the ventral visual stream,” *Proceedings of the National Academy of Sciences*, vol. 118, no. 3, p. e2014196118, 2021.
- [39] C. Zhuang, V. Xiang, Y. Bai, X. Jia, N. Turk-Browne, K. Norman, J. J. DiCarlo, and D. L. Yamins, “How well do unsupervised learning algorithms model human real-time and life-long learning?” in *Thirty-sixth Conference on Neural Information Processing Systems Datasets and Benchmarks Track*, 2022.
- [40] N. Carion, F. Massa, G. Synnaeve, N. Usunier, A. Kirillov, and S. Zagoruyko, “End-to-end object detection with transformers,” in *Proceedings of the European Conference on Computer Vision (ECCV)*. Springer, 2020, pp. 213–229.
- [41] X. Zhu, W. Su, L. Lu, B. Li, X. Wang, and J. Dai, “Deformable detr:

- Deformable transformers for end-to-end object detection," *arXiv preprint arXiv:2010.04159*, 2020.
- [42] A. Katharopoulos, A. Vyas, N. Pappas, and F. Fleuret, "Transformers are mms: Fast autoregressive transformers with linear attention," in *Proceedings of the 37th International Conference on Machine Learning (ICML)*, 2020, pp. 5156–5165.
- [43] A. Hassani, S. Walton, N. Shah, A. Abuduweili, J. Li, and H. Shi, "Escaping the big data paradigm with compact transformers," *arXiv preprint arXiv:2104.05704*, 2021.
- [44] W. Wang, E. Xie, X. Li, D. Fan, K. Song, D. Liang, T. Lu, P. Luo, and L. Shao, "Pyramid vision transformer: A versatile backbone for dense prediction without convolutions," *CoRR*, vol. abs/2102.12122, 2021.
- [45] Z. Liu, Y. Lin, Y. Cao, H. Hu, Y. Wei, Z. Zhang, S. Lin, and B. Guo, "Swin transformer: Hierarchical vision transformer using shifted windows," *CoRR*, vol. abs/2103.14030, 2021.
- [46] Y. Li, C. Wu, H. Fan, K. Mangalam, B. Xiong, J. Malik, and C. Feichtenhofer, "Mvitv2: Improved multiscale vision transformers for classification and detection," *2022 IEEE/CVF Conference on Computer Vision and Pattern Recognition (CVPR)*, pp. 4794–4804, 2021.
- [47] J.-g. Song, "Ufo-vit: High performance linear vision transformer without softmax," *arXiv preprint arXiv:2109.14382*, 2021.
- [48] J. Yang, C. Li, P. Zhang, X. Dai, B. Xiao, L. Yuan, and J. Gao, "Focal attention for long-range interactions in vision transformers," in *Proceedings of the International Conference on Neural Information Processing Systems (NeurIPS)*, vol. 34, 2021, pp. 30008–30022.
- [49] Y. Rao, W. Zhao, B. Liu, J. Lu, J. Zhou, and C.-J. Hsieh, "Dynamicvit: Efficient vision transformers with dynamic token sparsification," in *Proceedings of the International Conference on Neural Information Processing Systems (NeurIPS)*, vol. 34, 2021, pp. 13937–13949.
- [50] T. Chen, S. Kornblith, M. Norouzi, and G. Hinton, "A simple framework for contrastive learning of visual representations," in *International conference on machine learning*. PMLR, 2020, pp. 1597–1607.
- [51] K. He, H. Fan, Y. Wu, S. Xie, and R. Girshick, "Momentum contrast for unsupervised visual representation learning," in *Proceedings of the IEEE/CVF conference on computer vision and pattern recognition*, 2020, pp. 9729–9738.
- [52] M. Caron, H. Touvron, I. Misra, H. Jégou, J. Mairal, P. Bojanowski, and A. Joulin, "Emerging properties in self-supervised vision transformers," in *Proceedings of the IEEE/CVF international conference on computer vision*, 2021, pp. 9650–9660.
- [53] X. Chen, S. Xie, and K. He, "An empirical study of training self-supervised vision transformers," in *Proceedings of the IEEE/CVF International Conference on Computer Vision (ICCV)*, October 2021, pp. 9640–9649.
- [54] Y. Wu, L. Deng, G. Li, J. Zhu, and L. Shi, "Spatio-temporal backpropagation for training high-performance spiking neural networks," *Frontiers in neuroscience*, vol. 12, p. 331, 2018.
- [55] Y. Cao, Y. Chen, and D. Khosla, "Spiking deep convolutional neural networks for energy-efficient object recognition," *International Journal of Computer Vision*, vol. 113, no. 1, pp. 54–66, 2015.
- [56] E. Hunsberger and C. Eliasmith, "Spiking deep networks with lif neurons," *arXiv preprint arXiv:1510.08829*, 2015.
- [57] B. Rueckauer, I.-A. Lungu, Y. Hu, M. Pfeiffer, and S.-C. Liu, "Conversion of continuous-valued deep networks to efficient event-driven networks for image classification," *Frontiers in neuroscience*, vol. 11, p. 682, 2017.
- [58] J. Wu, C. Xu, X. Han, D. Zhou, M. Zhang, H. Li, and K. C. Tan, "Progressive tandem learning for pattern recognition with deep spiking neural networks," *IEEE Transactions on Pattern Analysis and Machine Intelligence*, vol. 44, no. 11, pp. 7824–7840, 2021.
- [59] Q. Meng, M. Xiao, S. Yan, Y. Wang, Z. Lin, and Z.-Q. Luo, "Training High-Performance Low-Latency Spiking Neural Networks by Differentiation on Spike Representation," *ArXiv preprint arXiv:2205.00459*, 2022.
- [60] Y. Wang, M. Zhang, Y. Chen, and H. Qu, "Signed neuron with memory: Towards simple, accurate and high-efficient ann-snn conversion," in *International Joint Conference on Artificial Intelligence*, 2022.
- [61] B. Han, G. Srinivasan, and K. Roy, "Rmp-snn: Residual membrane potential neuron for enabling deeper high-accuracy and low-latency spiking neural network," in *Proceedings of the IEEE/CVF Conference on Computer Vision and Pattern Recognition (CVPR)*, 2020, pp. 13558–13567.
- [62] R.-J. Zhu, Q. Zhao, and J. K. Eshraghian, "Spikegpt: Generative pre-trained language model with spiking neural networks," *arXiv preprint arXiv:2302.13939*, 2023.
- [63] J. H. Lee, T. Delbruck, and M. Pfeiffer, "Training deep spiking neural networks using backpropagation," *Frontiers in neuroscience*, vol. 10, p. 508, 2016.
- [64] S. B. Shrestha and G. Orchard, "Slayer: Spike layer error reassignment in time," in *Proceedings of the International Conference on Neural Information Processing Systems (NeurIPS)*, vol. 31, 2018.
- [65] C. Lee, S. S. Sarwar, P. Panda, G. Srinivasan, and K. Roy, "Enabling spike-based backpropagation for training deep neural network architectures," *Frontiers in neuroscience*, vol. 14, p. 119, 2020.
- [66] E. O. Neftci, H. Mostafa, and F. Zenke, "Surrogate gradient learning in spiking neural networks: Bringing the power of gradient-based optimization to spiking neural networks," *IEEE Signal Processing Magazine*, vol. 36, no. 6, pp. 51–63, 2019.
- [67] M. Xiao, Q. Meng, Z. Zhang, Y. Wang, and Z. Lin, "Training feedback spiking neural networks by implicit differentiation on the equilibrium state," vol. 34, 2021, pp. 14516–14528.
- [68] J. Zhang, B. Dong, H. Zhang, J. Ding, F. Heide, B. Yin, and X. Yang, "Spiking transformers for event-based single object tracking," in *Proceedings of the IEEE/CVF Conference on Computer Vision and Pattern Recognition (CVPR)*, 2022, pp. 8801–8810.
- [69] J. Zhang, L. Tang, Z. Yu, J. Lu, and T. Huang, "Spike transformer: Monocular depth estimation for spiking camera," in *Proceedings of the European Conference on Computer Vision (ECCV)*, 2022.
- [70] E. Mueller, V. Studenyak, D. Auge, and A. Knoll, "Spiking transformer networks: A rate coded approach for processing sequential data," in *2021 7th International Conference on Systems and Informatics (ICSAI)*. IEEE, 2021, pp. 1–5.
- [71] X. Chu, Z. Tian, Y. Wang, B. Zhang, H. Ren, X. Wei, H. Xia, and C. Shen, "Twins: Revisiting the design of spatial attention in vision transformers," in *Proceedings of the International Conference on Neural Information Processing Systems (NeurIPS)*, vol. 34, 2021, pp. 9355–9366.
- [72] H. Li, H. Liu, X. Ji, G. Li, and L. Shi, "Cifar10-dvs: an event-stream dataset for object classification," *Frontiers in neuroscience*, vol. 11, p. 309, 2017.
- [73] A. Krizhevsky, "Learning multiple layers of features from tiny images," 2009.
- [74] P. Gao, T. Ma, H. Li, Z. Lin, J. Dai, and Y. Qiao, "Mcmae: Masked convolution meets masked autoencoders," *Advances in Neural Information Processing Systems*, vol. 35, pp. 35632–35644, 2022.
- [75] K. Tian, Y. Jiang, qishuai diao, C. Lin, L. Wang, and Z. Yuan, "Designing BERT for convolutional networks: Sparse and hierarchical masked modeling," in *The Eleventh International Conference on Learning Representations*, 2023. [Online]. Available: <https://openreview.net/forum?id=NRxydtWup1S>
- [76] X. Zhang, Y. Tian, L. Xie, W. Huang, Q. Dai, Q. Ye, and Q. Tian, "Hivit: A simpler and more efficient design of hierarchical vision transformer," in *The Eleventh International Conference on Learning Representations*, 2023.
- [77] D. Zhou, B. Kang, X. Jin, L. Yang, X. Lian, Z. Jiang, Q. Hou, and J. Feng, "Deepvit: Towards deeper vision transformer," 2021.
- [78] A. Radford, J. W. Kim, C. Hallacy, A. Ramesh, G. Goh, S. Agarwal, G. Sastry, A. Askell, P. Mishkin, J. Clark, G. Krueger, and I. Sutskever, "Learning transferable visual models from natural language supervision," in *Proceedings of the 38th International Conference on Machine Learning*, ser. Proceedings of Machine Learning Research, M. Meila and T. Zhang, Eds., vol. 139. PMLR, 18–24 Jul 2021, pp. 8748–8763.
- [79] A. Kirillov, E. Mintun, N. Ravi, H. Mao, C. Rolland, L. Gustafson, T. Xiao, S. Whitehead, A. C. Berg, W.-Y. Lo, P. Dollár, and R. Girshick, "Segment anything," *arXiv:2304.02643*, 2023.
- [80] S. Bakhtiari, P. Mineault, T. Lillicrap, C. Pack, and B. Richards, "The functional specialization of visual cortex emerges from training parallel pathways with self-supervised predictive learning," *Advances in Neural Information Processing Systems*, vol. 34, pp. 25164–25178, 2021.
- [81] J. Millet, C. Caucheteux, Y. Boubenec, A. Gramfort, E. Dunbar, C. Pallier, J.-R. King *et al.*, "Toward a realistic model of speech processing in the brain with self-supervised learning," *Advances in Neural Information Processing Systems*, vol. 35, pp. 33428–33443, 2022.
- [82] N. Rathi, G. Srinivasan, P. Panda, and K. Roy, "Enabling deep spiking neural networks with hybrid conversion and spike timing

- dependent backpropagation," *arXiv preprint arXiv:2005.01807*, 2020.
- [83] T. Bu, W. Fang, J. Ding, P. DAI, Z. Yu, and T. Huang, "Optimal ANN-SNN conversion for high-accuracy and ultra-low-latency spiking neural networks," in *International Conference on Learning Representations*, 2022. [Online]. Available: https://openreview.net/forum?id=7B3JMM1k_M
- [84] Y. Hu, Q. Zheng, X. Jiang, and G. Pan, "Fast-snn: Fast spiking neural network by converting quantized ann," *arXiv preprint arXiv:2305.19868*, 2023.
- [85] Z. Hao, J. Ding, T. Bu, T. Huang, and Z. Yu, "Bridging the gap between ANNs and SNNs by calibrating offset spikes," in *The Eleventh International Conference on Learning Representations*, 2023. [Online]. Available: <https://openreview.net/forum?id=PFbzoWZyZRX>
- [86] S. Deng, Y. Li, S. Zhang, and S. Gu, "Temporal Efficient Training of Spiking Neural Network via Gradient Re-weighting," in *International Conference on Learning Representations (ICLR)*, 2021.
- [87] M. Yao, G. Zhao, H. Zhang, Y. Hu, L. Deng, Y. Tian, B. Xu, and G. Li, "Attention spiking neural networks," *IEEE Transactions on Pattern Analysis and Machine Intelligence*, 2023.
- [88] M. Yao, J. Hu, Z. Zhou, L. Yuan, Y. Tian, B. Xu, and G. Li, "Spike-driven transformer," *arXiv preprint arXiv:2307.01694*, 2023.
- [89] C. Zhou, L. Yu, Z. Zhou, H. Zhang, Z. Ma, H. Zhou, and Y. Tian, "Spikingformer: Spike-driven residual learning for transformer-based spiking neural network," *arXiv preprint arXiv:2304.11954*, 2023.
- [90] D. P. Kingma and J. Ba, "Adam: A method for stochastic optimization," in *International Conference on Learning Representations, ICLR*, 2015.
- [91] E. D. Cubuk, B. Zoph, J. Shlens, and Q. Le, "Randaugment: Practical automated data augmentation with a reduced search space," in *Neural Information Processing Systems, NeurIPS*, 2020.
- [92] Z. Zhong, L. Zheng, G. Kang, S. Li, and Y. Yang, "Random erasing data augmentation," in *Association for the Advancement of Artificial Intelligence, AAAI*, 2020, pp. 13 001–13 008.
- [93] G. Huang, Y. Sun, Z. Liu, D. Sedra, and K. Q. Weinberger, "Deep networks with stochastic depth," in *European Conference on Computer Vision, ECCV*, B. Leibe, J. Matas, N. Sebe, and M. Welling, Eds., vol. 9908, 2016, pp. 646–661.
- [94] H. Zhang, M. Cissé, Y. N. Dauphin, and D. Lopez-Paz, "mixup: Beyond empirical risk minimization," in *International Conference on Learning Representations, ICLR*, 2018.
- [95] S. Yun, D. Han, S. Chun, S. J. Oh, Y. Yoo, and J. Choe, "Cutmix: Regularization strategy to train strong classifiers with localizable features," in *International Conference on Computer Vision, ICCV*, 2019, pp. 6022–6031.
- [96] N. Rathi and K. Roy, "Diet-snn: Direct input encoding with leakage and threshold optimization in deep spiking neural networks," *arXiv preprint arXiv:2008.03658*, 2020.
- [97] Y. Wu, L. Deng, G. Li, J. Zhu, Y. Xie, and L. Shi, "Direct Training for Spiking Neural Networks: Faster, Larger, Better," in *Proceedings of the AAAI Conference on Artificial Intelligence (AAAI)*, 2019, pp. 1311–1318.
- [98] W. Zhang and P. Li, "Temporal spike sequence learning via backpropagation for deep spiking neural networks," in *Proceedings of the International Conference on Neural Information Processing Systems (NeurIPS)*, vol. 33, 2020, pp. 12 022–12 033.
- [99] Y. Li, Y. Kim, H. Park, T. Geller, and P. Panda, "Neuromorphic data augmentation for training spiking neural networks," in *European Conference on Computer Vision*. Springer, 2022, pp. 631–649.
- [100] Z. Wu, H. Zhang, Y. Lin, G. Li, M. Wang, and Y. Tang, "LIAF-Net: Leaky Integrate and Analog Fire Network for Lightweight and Efficient Spatiotemporal Information Processing," *IEEE Transactions on Neural Networks and Learning Systems*, pp. 1–14, 2021.
- [101] A. Kugele, T. Pfeil, M. Pfeiffer, and E. Chicca, "Efficient Processing of Spatio-temporal Data Streams with Spiking Neural Networks," *Frontiers in Neuroscience*, vol. 14, p. 439, 2020.
- [102] J. Kaiser, H. Mostafa, and E. Neftci, "Synaptic Plasticity Dynamics for Deep Continuous Local Learning (DECOLLE)," *Frontiers in Neuroscience*, vol. 14, p. 424, 2020.
- [103] Y. Li, Y. Guo, S. Zhang, S. Deng, Y. Hai, and S. Gu, "Differentiable Spike: Rethinking Gradient-Descent for Training Spiking Neural Networks," in *Proceedings of the International Conference on Neural Information Processing Systems (NeurIPS)*, vol. 34, 2021, pp. 23 426–23 439.
- [104] Y. Kim and P. Panda, "Optimizing Deeper Spiking Neural Networks for Dynamic Vision Sensing," *Neural Networks*, vol. 144, pp. 686–698, 2021.